Monthly Notices
of the
ROYAL ASTRONOMICAL SOCIETY

MNRAS **479,** 5035–5048 (2018)
Advance Access publication 2018 June 18

doi:10.1093/mnras/sty1614

Evolved stars in the Local Group galaxies – II. AGB, RSG stars, and dust production in IC10

F. Dell'Agli,[1,2]★ M. Di Criscienzo,[3] P. Ventura,[3] M. Limongi,[3]
D. A. García-Hernández,[1,2] E. Marini[3,4] and C. Rossi[5]

[1]*Instituto de Astrofísica de Canarias (IAC), E-38200 La Laguna, Tenerife, Spain*
[2]*Departamento de Astrofísica, Universidad de La Laguna (ULL), E-38206 La Laguna, Tenerife, Spain*
[3]*INAF – Osservatorio Astronomico di Roma, Via Frascati 33, 00040, Monte Porzio Catone (RM), Italy*
[4]*Dipartimento di Matematica e Fisica, Universita degli Studi 'Roma Tre', Via della Vasca Navale 84, I-00146 Roma, Italy*
[5]*Dipartimento di Fisica, Università di Roma 'La Sapienza', P.le Aldo Moro 5, 00143, Roma, Italy*

Accepted 2018 June 11. Received 2018 June 11; in original form 2018 May 15

ABSTRACT

We study the evolved stellar population of the Local Group galaxy IC10, with the aim of characterizing the individual sources observed and to derive global information on the galaxy, primarily the star-formation history and the dust production rate. To this aim, we use evolutionary sequences of low- and intermediate-mass ($M < 8\,M_{\odot}$) stars, evolved through the asymptotic giant branch phase, with the inclusion of the description of dust formation. We also use models of higher mass stars. From the analysis of the distribution of stars in the observational planes obtained with infrared bands, we find that the reddening and distance of IC10 are $E(B-V) = 1.85$ mag and $d = 0.77$ Mpc, respectively. The evolved stellar population is dominated by carbon stars that account for 40 per cent of the sources brighter than the tip of the red giant branch. Most of these stars descend from $\sim$1.1–1.3 $M_{\odot}$ progenitors, formed during the major epoch of star formation, which occurred $\sim$2.5 Gyr ago. The presence of a significant number of bright stars indicates that IC10 has been the site of significant star formation in recent epochs and currently hosts a group of massive stars in the core helium-burning phase. Dust production in this galaxy is largely dominated by carbon stars; the overall dust production rate estimated is $7 \times 10^{-6}\,M_{\odot}\,yr^{-1}$.

Key words: stars: abundances – stars: AGB and post-AGB.

1 INTRODUCTION

Dwarf galaxies are the dominant component among the structures populating the Local Group (LG). They are characterized by a significant diversity in terms of structural properties, star-formation history (SFH), and metal enrichment (see e.g. Weisz et al. 2014). The understanding of the origin of these heterogeneities proves crucial for a number of astrophysical contexts, ranging from pure stellar evolution grounds to some fundamental aspects regarding the formation and the evolution of galaxies.

Among the dwarf galaxies in the LG IC10 is one of the most interesting systems, given its large total mass ($\log(M/M_{\odot}) \sim 8.5$; Vaduvescu, McCall & Richer 2007), which makes it one of the most massive and luminous dwarfs. Furthermore, the large H α luminosity (e.g. Mateo 1998; Kennicutt et al. 2008; Tehrani, Crowther & Archer 2017) and the very large density of Wolf-Rayet stars (Massey, Armandroff & Conti 1992; Massey & Armandroff 1995; Massey & Holmes 2002), a factor $\sim$20 higher than in the Large Magellanic Cloud (hereafter LMC), suggest that IC10 is currently experiencing vigorous star formation.

Sanna et al. (2008a, 2009) used *Hubble Space Telescope* (*HST*) data to derive the distance of IC10 (distance modulus $\mu = 24.60 \pm 0.15$ mag), based on the magnitude of the tip of the red giant branch (hereafter TRGB); the authors also investigated the age and metallicity distribution by comparing Hubble's Advanced Camera for Surveys (ACS) and WFPC2 data with results from evolutionary calculations of main sequence, red giant and horizontal branch stars. A complementary approach to reconstruct the history of the star formation in IC10 was followed by Magrini & Goncalves (2009), based on its planetary nebulae (PNe) and H II region populations. The first uniform derivation of 40 LG dwarf galaxies SFHs was recently presented by Weisz et al. (2014), based on analysis of colour–magnitude diagrams constructed from archival *HST*/WFPC2 imaging. IC10 was part of this study, where the main peak of the SFH is found around 1.5–4 Gyr, followed by a significant star-formation rate (SFR) even in the most recent epoch ($\sim$400 Myr and 10 Myr).

★ E-mail: fdellagli@iac.es

All these results clearly evidence the suitability of IC10 as excellent target to study the evolved population in dwarf galaxies. A detailed analysis is now possible thanks to the significant improvements in the modelling of the asymptotic giant branch (AGB) phase of stars of low and intermediate mass. Indeed, the description of the stellar structure has been completed in recent times with the modelling of the dust formation in the circumstellar envelopes (Ventura et al. 2012a,b, 2014; Nanni et al. 2013, 2014), a key ingredient to interpret infrared (IR) data of cool stars.

The comparison between IR data and AGB models which consider dust formation proved useful in several studies aimed at understanding the properties of dust-enshrouded objects in the Magellanic Clouds (MCs) (e.g. Boyer et al. 2015c; Kraemer et al. 2017). Recent studies used star + dust systems to characterize the entire AGB population of the MCs, in terms of mass, age, and metallicity distribution (Dell'Agli et al. 2014, 2015a,b; Nanni et al. 2017). These studies turned out to be extremely useful not only to interpret the observed stellar population but also to infer important information regarding the efficiency of some chemical phenomena driving the evolution through the AGB phase, the modality with which dust formation occurs and the absorption and scattering properties of the most relevant dust species formed in the AGB winds (Ventura et al. 2015a, 2016; Nanni et al. 2016).

While the MCs have so far been proved to be the best laboratories to study the AGB phase, owing to their low reddening and known distances, the increasing availability of high-quality data in other LG galaxies will soon allow a better understanding of the main properties of AGB stars. An exhaustive analysis of the evolution of this class of objects demands that further environments external to the MCs are explored; this is even more important, given the forthcoming launch of the *James Webb Space Telescope* (*JWST*), which will make available data of thousands of AGB stars from several galaxies in the LG. The opportunities offered by the *JWST* mission for these studies are discussed in Jones et al. (2017).

Early attempts to use IR data to derive information on the evolved population of environments beyond the MCs were done, e.g. for M33 (Javadi et al. 2017), NGC 147, and NGC 185 (Hamedani Golshan et al. 2017). In a study focused on the evolved stellar population of IC 1613, Dell'Agli et al. (2016) interpreted the AGB stars of this galaxy, providing a characterization of the sources observed, in terms of mass, chemical composition, and formation epoch of the progenitors.

In this work, we apply the same approach used in Dell'Agli et al. (2016) to study the evolved population of IC10. This is possible thanks to the combined availability of near-infrared (NIR) data published by Gerbrandt, McConnachie & Irwin (2015), and of *Spitzer* mid-infrared data by the survey of Dust in Nearby Galaxies with *Spitzer* (DUSTINGS; Boyer et al. 2015a,b). We carry out a statistical analysis of the distribution of stars in the colour–colour and colour–magnitude planes (obtained with various combinations of NIR and mid-IR *Spitzer* filters) to refine the SFH, allowing the best compatibility between models and observations. We show how this methodology also allows the determination of the reddening and the distance of the galaxy. To our knowledge, in the context of the interpretation of evolved and dusty populations, this is the first work that considers the possible contamination from RSG stars in the regions of the observational planes populated by AGB stars. This issue is particularly relevant in a starburst galaxy such as IC10.

The paper is organized as follows: Section 2 is devoted to present the observational sample considered; the stellar evolution and dust formation models are briefly described in Section 3; and the main properties of the AGB stars used in this work are discussed in Section 4. In Section 5, we describe the construction of the synthetic population, the comparison of the observed, and the expected distribution of the evolved stars in different colour–colour and colour–magnitude planes, in order to find the reddening and the distance and to reconstruct the SFH of the galaxy. The characterization of the evolved stellar population of IC10 is addressed in Section 6, while the most obscured sources are described in Section 7. Section 8 is dedicated to describe the dust produced by AGB stars in IC10 and to estimate the overall dust production rate (DPR) of the galaxy; the PNe population of IC10, specifically the objects for which both the nitrogen and oxygen abundances have been determined, is interpreted in Section 9. Finally, the conclusions are given in Section 10.

2 OBSERVATIONAL SAMPLES

To perform a quantitative analysis of the evolved stellar population of IC10, we rely on the most complete samples of stars available in the literature. We focus our attention on the NIR and mid-IR wavelength range, where the emission for the majority of these stars peaks.

Gerbrandt et al. (2015) provided J, H, and K data for a wide sample of stars in IC10 within an area of 0.75 deg^2, using the Wide Field Camera on the 3.8m United Kingdom Infrared Telescope, during a single observing run. Moreover, the DUSTiNGS survey (Boyer et al. 2015a) was specifically designed to identify dust-producing AGB stars, made available mid-IR magnitudes for hundreds of stars in dwarf galaxies in the LG. Among the others, IC10 has been observed with the InfraRed Array Camera in the [3.6] and [4.6] filters during two epochs to reduce the effects of variability.

The wide opportunities offered by the simultaneous analysis of NIR and mid-IR data to study evolved stars and to distinguish different classes of objects were explored in a series of works (Boyer et al. 2011; Woods et al. 2011; Donald et al. 2012). This approach was also used by Dell'Agli et al. (2016) to understand the distribution and extension of the evolved stellar population of IC1613 in various observational planes. In particular, in the colour–magnitude ($K - [4.5]$, [4.5]) plane, carbon- and oxygen-rich stars occupy well-defined and distinct regions. An important outcome of the study by Dell'Agli et al. (2016) is that the analysis of the distribution of stars in this plane allows to infer useful constrains on the SFH of the galaxy during the last Gyr and the characterization of the dust produced by the individual sources.

In order to carry out a similar analysis in IC10, we first homogenized the two astrometries by applying a corrective factor based on the brightest stars of both catalogues; we then cross-correlated the Gerbrandt et al. (2015) and Boyer et al. (2015a) samples, using a matching radius of 1.2 arcsec, which is the largest spatial resolution of Spitzer; when multiple matches occurred, only the closest match with the brightest star was kept.

From the analysis described in Sections 5.2 and 5.3, we found and adopt a distance of 0.77 Mpc and reddening $E(B - V) = 1.14$ mag, values in the range of the latest estimates from the literature (e.g. Richer et al. 2001; Demers, Battinelli & Letarte 2004; Sanna et al. 2008a,b).

The final sample is composed of 20399 sources. Fig. 1 shows the distribution of the stars in this sample, indicated as grey points, in the ($K - [4.5]$, [4.5]) colour–magnitude plane, to which we will refer hereafter as CMD. In order to clean the sample from the majority of the foreground objects, in the following analysis we will consider stars with only $(J - H)_0 > 0.7$ mag, which, according to Gerbrandt et al. (2015), removes about 96 per cent of all the

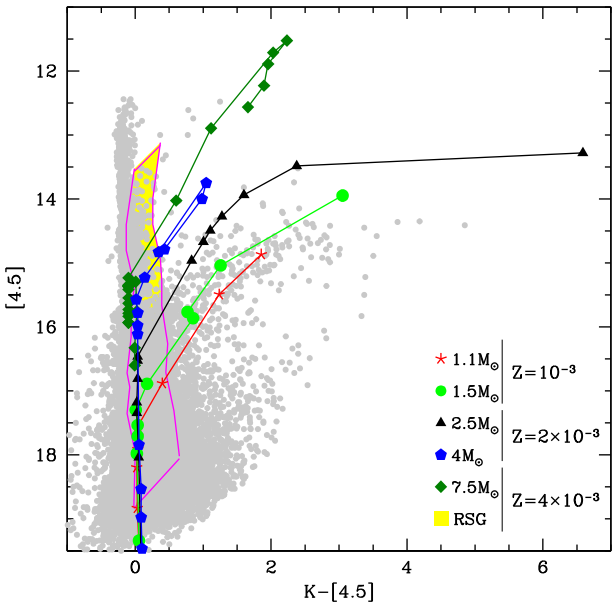

Figure 1. The evolutionary tracks of stars of various mass and metallicity are overimposed to the observations in the colour–magnitude ($K - [4.5]$, [4.5]) plane. The yellow region, delimited by a magenta track, points the locus of the plane populated by stars of mass in the range 6–20 $M_\odot$ during the core helium-burning phase. See the text for the choices regarding the assumed reddening and distance of IC10.

foreground contaminants. The removal of a small fraction of genuine IC10 stars by this cut makes no difference to the subsequent analysis. We will also exclude all the stars with $K_0 > 18.3$ mag to limit the present analysis to the stars brighter than the TRGB. With these assumptions, we obtain a final sample composed of ∼3680 objects. A detailed comparison between our theoretical expectations and the observations in this plane is presented in Section 6.

To prevent the possibility that we miss a large fraction of the objects with the highest degree of obscuration, which we expect to have extremely faint K magnitudes, we take into account the stars identified as 'extreme' (xAGB) by Boyer et al. (2015b). These sources, included in the *Spitzer* sample previously described, were classified on the basis of their variability and of their red ($[3.6] - [4.5] > 0.1$) colours. Among all the galaxies investigated within DUSTiNGS, IC10 harbours the largest population of extreme stars. The chemical composition of these stars is unknown, thus their study is important to deduce the main properties of the progenitors. Furthermore, considering their large IR emission, suggesting significant dust production in their circumstellar envelopes, the characterization of these objects proves crucial to determine the overall DPR in IC10. While this choice allows us to provide a robust evaluation of the global DPR, we believe important here to underline that the present analysis might likely provide a lower limit of this quantity, as a paucity of extremely obscured stars, similar to those observed in the LMC by Gruendl et al. (2008), with very low fluxes in the spectral region around 4.5 μm, might not be present in the Boyer et al. (2015b) sample.

The study by Boyer et al. (2015b) has been recently completed by Boyer et al. (2017), who presented a follow-up survey with WFC3/IR on the *HST*, and identified a total of ∼26 dusty M-type stars, most of which belong to IC10. These stars, characterized by a large IR excess, with IR colours up to $[3.6] - [4.5] \sim 1$, are mostly confined in the inner regions of the galaxy, suggesting that they are more massive than the dominant C-rich obscured population.

Finally, Lebouteiller et al. (2012) characterized stars in IC10 by their silicate dust features to identify O-rich stars and to distinguish between AGB and RSG stars. The detection of the silicate dust features was based on the mid-IR spectra obtained with the IR Spectrograph (IRS) onboard of *Spitzer*.

The discussion of all these samples on the basis of our synthetic population is presented in Section 7. Before addressing the characterization of the individual sources observed, we briefly present the evolutionary models adopted for the analysis and we discuss the reddening, distance, and SFH of IC10, which allow the best agreement between the observational evidence and the theoretical framework.

3 MODELLING THE AGB PHASE WITH DUST FORMATION AND RSG STARS

To investigate the evolved stellar population of IC10, we consider models of stars with initial masses in the range 0.8–8 $M_\odot$ and metallicity[1] $Z = 1, 2, 4 \times 10^{-3}$. The upper limit in mass is due to the ignition of carbon burning in stars of mass above 8 $M_\odot$; these stars will finally undergo core collapse, without evolving through the AGB phase.

The models used here are presented and discussed in Dell'Agli et al. (2016), where all the details of the AGB evolution and dust-formation modelling are given. The description of the AGB phase is essentially made up of three different steps: (a) the modelling of the AGB evolution, via the code ATON (Ventura et al. 1998); (b) we describe the dust-formation process for some evolutionary phases chosen along the AGB, by means of the schematization by the Heidelberg group (Ferrarotti & Gail 2006), which was applied by Ventura et al. (2012a,b, 2014); and (c) the IR colours are obtained based on the values of the physical quantities of the star and on the dust present in the envelope by means of the DUSTY code (Nenkova, Ivezić & Elitzur 1999).

We believe important to stress here that to undertake this kind of analysis, based on the interpretation of observations in the near- and mid-IR spectral region, the description of the dust-formation process is mandatory, because the IR emission by the star is determined by the number density and the grain-size distribution of the dust particles formed in the circumstellar envelope.

This having said, we remind that the present generation of AGB + dust models must be considered as a preliminary step towards a more physically sound description, considering that the description proposed by Ferrarotti & Gail (2006) is based on a grey treatment of extinction and neglects the effects of pulsation, which might affect the results obtained significantly (Bladh & Höfner 2012; Bladh et al. 2013, 2015, 2017). More important, the rate of mass loss in these models is assumed a priori and thus it is not a consequence of the dust-formation process; this makes the results obtained critically dependent of the description of mass loss, which affects significantly both the main properties of AGB evolution (Karakas & Lattanzio 2014) and the formation of dust (Ventura et al. 2014). The choice of the optical constants also plays an important role, as shown, e.g.

[1]We indicate with Z the mass fraction of all the species but hydrogen and helium present initially in the star, thus characterizing the mixture of the gas from which the stars formed. Note that the overall metallicity increases during the AGB phase of the stars exposed to carbon enrichment in the surface layers.

in Nanni et al. (2016). Finally, the present description assumes that the wind expands isotropically from the surface of single stars, thus neglecting the effects of the presence of a companion, confirmed by recent analysis of resolved AGB stars (Ramstedt et al. 2014; Richards et al. 2014; Rau et al. 2015).

Consistently with the previous works on this argument, we will quantify the degree of obscuration of the stars by the optical depth at 10 μm, τ_{10}, which is determined by the radial distribution of the dust particles in the surroundings of the star (see Section 2.3 in Dell'Agli et al. 2015a).

As stated in the Introduction Section, because IC10 is a starbust galaxy, we considered the presence of RSGs in the sample observed. Stars with masses $M \sim 6$–$20\,M_{\odot}$ evolve on time-scales shorter than 70 Myr and during the helium-burning phase evolve at luminosities in the range $3 \times 10^3 - 1.4 \times 10^5\,L_{\odot}$. During the red part of the loop characterizing the core helium-burning phase, the position of these objects in the colour–magnitude diagram partly overlaps with AGB stars. To give an estimate of the contamination from RSG stars, we considered the core helium-burning phase of the models mentioned earlier in this section, presented in Dell'Agli et al. (2016), with mass in the range 6–8 $M_{\odot}$. The RSG evolution of stars with masses $M \geq 9\,M_{\odot}$ was described by means of the rotating version of the FRANEC code (the interested reader is referred to Chieffi & Limongi (2013) for more details).

Given the uncertainties related to the mass loss and the dust production mechanisms in the winds of this class of objects, it is not possible to clearly model the distribution of these stars in the colour–magnitude diagrams. We tentatively assumed a variety of degrees of obscuration, described by optical depths in the range $0 < \tau_{10} < 0.2$. Recently, Groenewegen & Sloan (2018) estimate $\tau_{0.5}$ for ∼20 supergiant stars in the SMC, fitting the SEDs and IRS spectra with a dust radiative-transfer model. Their results are in agreement with the degrees of obscuration adopted in this work. This adds more robustness to our assumption, considering the similarity in the metallicity of distribution of stars in IC10 and in the SMC. While the presence of heavily obscured RSG stars cannot be completely ruled out (e.g. Jones et al. 2015; Goldman et al. ; Groenewegen & Sloan 2018), this conservative assumption on the range of τ_{10} values reached by core helium-burning stars allows us to identify a region in the CMD (indicated with a yellow shading delimited by magenta lines in Fig. 1), where we expect that most (if not all) of these stars are found.

4 AGB STARS: EVOLUTION PROPERTIES AND IR COLOURS

The most recent and complete study of the SFH of IC10 is provided by Weisz et al. (2014); we consider their results as a starting point to compute the synthetic population of evolved stars. According to Weisz et al. (2014), the main peak of the SFH occurred around 1.5–4 Gyr ago, when low-mass stars of metallicity $Z \sim 10^{-3}$ formed. These are the progeny of most of the AGB population currently evolving in IC10. We describe here their main properties, as they evolve through the AGB phase, to ease the interpretation of the observed distribution of stars in the colour–colour and colour–magnitude planes.

Before entering the discussion of the evolutionary properties, we believe important to stress that the description of the AGB phase of these stars, of initial mass below ∼3 $M_{\odot}$, is fairly robust. This is the result, which holds for various metallicities, shown in a series of recent papers (Ventura et al. 2016, 2018). Conversely, the modelling of their higher mass counterparts is more uncertain, as it is heavily affected by the modelling of the convective instability (Ventura et al. 2015a, 2018).

The two top panels of Fig. 2 show the variation of the luminosity and of the C/O ratio during the TP-AGB phase[2] of stellar models of metallicity $Z \leq 2 \times 10^{-3}$ and mass in the range 1–2.5 $M_{\odot}$. In the abscissa, we indicate the time, counted since the first thermal pulse. For clarity reasons, we report only the values of the physical quantities referring to an evolutionary stage in the middle of each interpulse phase, chosen in conjunction with the maximum luminosity.

The stars reported in Fig. 2 evolve through the two major phases of core H- and He-burning, with time-scales between 400 Myr and 6 Gyr. Fig. 2 shows that the overall duration of the TP-AGB phase is in the range of 1–2 Myr and follows a trend that is not monotonic with mass. For stars with mass below ∼2 $M_{\odot}$, the evolution time grows with the stellar mass because the higher the mass, the longer the time required to eject the external envelope. On the other hand, in the mass domain $M > 2\,M_{\odot}$, the most relevant factor is that more massive stars evolve to obtain bigger cores and larger luminosities, which makes the duration of the AGB phase shorter. This behaviour was thoroughly described by Ventura et al. (2016), where the interested reader can also find a discussion regarding the uncertainties of the evolutionary time-scales.

In the top, left-hand panel of Fig. 2, we also show the luminosity of the TRGB (∼2200 $L_{\odot}$), obtained by following the RGB evolution of low-mass models sharing the same chemical composition of the AGB models, until the helium flash. Most of the stars evolve at luminosities fainter than the TRGB during the evolutionary phases preceding the TP-AGB; the only exception is the ∼2.5 $M_{\odot}$ star, which is brighter than the TRGB for a limited part of the EAGB evolution. This is important for the scope of this work because it allows us to use solely data of stars brighter than the TRGB.

A common property of the stars in this mass domain is the achievement of the carbon-star stage, as a consequence of a series of third-dredge up (TDU) episodes (see top, right-hand panel of Fig. 2). Given the relatively small initial oxygen content, the C/O > 1 condition is reached after a few TPs, so that the duration of the C-star phase is approximately half the overall duration of the TP-AGB evolution. The final C/O, in the range of 10–50, increases with the initial mass of the star, because stars of higher mass experience a higher number of TDU events before the envelope is entirely lost (Ventura et al. 2014).

The amount of carbon accumulated in the external layers of the star, particularly the excess of carbon with respect to oxygen, is of extreme importance for the dust production in the circumstellar envelope (Ferrarotti & Gail 2006; Lagadec & Zijlstra 2008; Groenewegen et al. 2007, 2009). The increase in the surface carbon favours the formation of considerable quantities of solid carbon grains, which grow bigger and bigger as the wind expands from the surface of the star (Ferrarotti & Gail 2006; Dell'Agli et al. 2015a,b; Ventura et al. 2016). This is accompanied by the shift towards longer wavelengths of the stellar spectrum, owing to the reprocessing of the radiation emitted by the central star by the dust particles present in the wind.

Since the SED shifts to the red when the C/O > 1 condition is reached, the duration of the evolutionary phase during which the

[2]We generally refer to AGB to describe the evolutionary phases that follow the end of core helium burning. We use the terminology TP-AGB to address the part of the AGB evolution following the first thermal pulse. The AGB phases preceding the first thermal pulse are called early-AGB (EAGB).

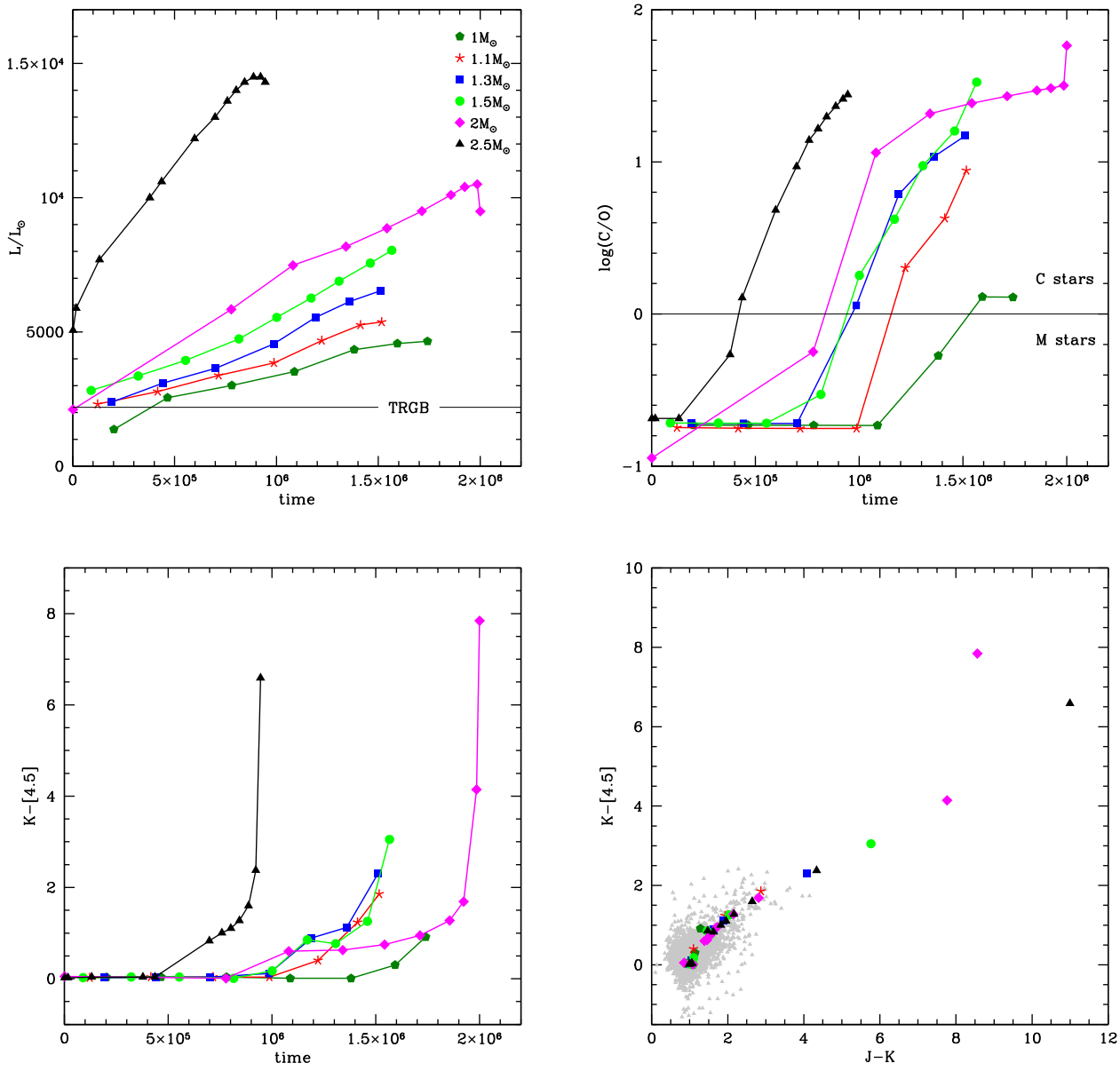

Figure 2. The evolution of the luminosity (top, left-hand panel) and of the C/O ratio (top, right-hand panel) of 1–2 $M_\odot$ at $Z = 10^{-3}$ and 2.5 $M_\odot$ at $Z \leq 2 \times 10^{-3}$. The thin, horizontal lines mark the location of the TRGB and the boundary between M stars and carbon stars. The variation of the (K-[4.5]) colour is shown in the bottom, left-hand panel. We also show the excursion of the tracks in the colour–colour (J-K) versus (K-[4.5]) plane, overimposed to the data of the IC10-evolved stellar population by Gerbrandt et al. (2015) and Boyer et al. (2015a). The adopted reddening is $E(B - V) = 1.14$ mag (see Section 5.2).

colours are reddest is extremely short; this is because the formation of great quantities of dust is accompanied by a significant increase in the rate of mass loss, which provokes a fast consumption of the external mantle, halting the TP-AGB evolution (Ventura et al. 2016).

The gradual shift to the IR of the SED of the stars is also clear in the bottom, right-hand panel of Fig. 2, which shows the evolution of the stars in the colour–colour (J−K, K-[4.5]) plane. For clarity reasons, we show only the theoretical tracks of $M \leq 2.5\,M_\odot$ stars in the bottom, right-hand panel of Fig. 2. As stated earlier in this section, the vast majority of the AGB population of IC10 is made up of the progeny of these stars; we will return to this point in the following sections. The sequences of the various low-mass stars cannot be distinguished on this plane, if not for the extension of the track, which changes according to the amount of dust formed, hence on the amount of carbon accumulated in the surface regions.

Because the duration of the phase with the largest IR emission is only a small fraction of the entire AGB life, for most of the time the stars evolve at approximately constant IR colours, namely $J - K \sim 1$ and $K - [4.5] \sim 0$. The shift to the red of the SED occurs only in the late TP-AGB phases, after a significant enrichment in the surface carbon occurs (see the bottom, left-hand panel of Fig. 2).

In summary, the most important points relevant to our analysis are:

(i) All the stars of mass above $\sim$1 $M_\odot$ evolve through phases characterized by a significant degree of obscuration of the stellar spectrum, with IR colours up to $J - K \sim 4$ and $K - [4.5] \sim 2.5$, or even larger in same cases. The K-magnitude spread of sources

reaching these colours can be used as an indicator of the duration of the star-forming phase for ages in the range 400 Myr–6Gyr, because stars of different mass, which formed in different epochs, reach the largest degree of obscuration towards the final evolutionary phases at different luminosities (see top, left-hand panel of Fig. 2).

(ii) All the stars spend most of the AGB evolution with IR colours $J - K \sim 1$ and $K - [4.5] \sim 0$. On the colour-colour (J-K, K-4.5) diagram, this is expected to produce a clump of objects around the aforementioned values, which represent the locus of stars with negligible amounts of dust in their circumstellar envelope.

(iii) The higher is the initial mass of the star, the more extended to the red is the evolutionary track. In particular, it is extremely important to check for the presence of objects with $J - K > 4$ and $K - [4.5] > 2.5$. While single stars just entered in the superwind phase or systems surrounded by an optically thick circumbinary disk can evolve to such red colours, the detection of a significant number of sources with such red $J - K$ and $K - [4.5]$ would imply the presence of a large number of stars of mass above $2\,M_{\odot}$, suggesting that the epoch around ∼500 Myr was characterized by a high rate of star formation. The presence of a relatively large number of these stars in the LMC was invoked by Dell'Agli et al. (2014, 2015a) to explain the detection of stars with a very large degree of obscuration, with IR colours $[3.6] - [4.5] \sim 3$.

5 IC10: THE DETERMINATION OF REDDENING, DISTANCE, AND SFH FROM IR OBSERVATIONS

5.1 Synthetic population

To study IC10, we use the same method adopted to interpret IR observations of the LMC (Dell'Agli et al. 2015a), SMC (Dell'Agli et al. 2015b), and IC 1613 (Dell'Agli et al. 2016). This approach is based on the AGB and RSG models presented and discussed in Sections 3 and 4. We assume a metal-poor chemistry, with $Z = 10^{-3}$, for ages above 1.5 Gyr, which reflects into masses below $\sim 2\,M_{\odot}$. For stars younger than 200 Myr (i.e. masses above $\sim 4\,M_{\odot}$), we assume $Z = 4 \times 10^{-3}$; an intermediate metallicity, $Z = 2 \times 10^{-3}$, is adopted for the stars formed between 200 Myr and 1.5 Gyr ago.

Based on the AGB+core helium-burning models, we generate the synthetic distribution of stars in the different observational planes to compare with the observations. To do this, we extract randomly a number of stars in the various epochs, according to the values of the SFR and of the mass function. For the latter, we assume a Salpeter law, with index $x = -1.3$ (Salpeter 1955). This choice has no effects on the results obtained.

5.2 The reddening of IC10

IC10 is located in the outskirts of the LG at low Galactic latitude ($b = -3.3°$); this renders the determination of reddening rather uncertain. The values reported by Demers et al. (2004) span the range from $E(B - V) = 0.40$ mag to $E(B - V) = 1.85$ mag. More recent results in the literature give $E(B - V) = 0.78$ mag (Sanna et al. 2008b) and $E(B - V) = 0.98$ mag (Kim et al. 2009).

We base our choice on the results shown in the bottom, right-hand panel of Fig. 2 and discussed in point (ii) of the previous section: the great majority of low-mass stars populate the region of the CCD centred at $(J - K, K - [4.5]) = (1, 0)$. We underline that this is independent of the dust model adopted. Therefore, we shifted the observed points on the CCD to make the most populated region to be at $(J - K, K - [4.5]) = (1, 0)$. This method allowed us to deduce the reddening, which is found to be $E(B - V) = 1.14$ mag, in agreement with the analysis by Sakai, Madore & Freedman (1999), based on the study of the Cepheids in IC10. This result is also consistent with Schlafly & Finkbeiner (2011), who find $E(B - V) = 1.13$ mag for the central 5′ of IC10.

5.3 The distance of IC10

A list of published estimates of the distance of IC10, most in the range 0.7–0.8 Mpc, is given in Demers et al. (2004). More recent estimates have been provided by Vacca, Sheehy & Graham (2007), Kim et al. (2009), and Gonçalves et al. (2012). In this analysis, we base the determination of the distance on the position in the CMD of the stars with the largest degree of obscuration. These objects, as shown in Fig. 1, are located in the right side of the plane and correspond to the late AGB phases of C-stars, reached by stars with initial mass in the range 1–2.5 $M_{\odot}$. As discussed in the previous section, AGB modelling can provide reliable estimates of their luminosities. These determinations of the bolometric magnitudes allow us to predict the position of these stars in the CMD, for various degrees of obscuration, in turn related to the values of the optical depth. Accordingly, the locus of C-stars will define a diagonal band in the CMD, extending from $K - [4.5] \sim 0$ to the red side of the plane. The details of the SFH affect the relative distribution of stars across this band but have practically no influence on the $K - [4.5]$ versus $[4.5]$ trend.

To determine the distance of IC10, we shifted vertically the set of the theoretical tracks corresponding to 1–2.5 $M_{\odot}$ stars (see Fig. 1), until a reasonable overlapping with the observed sources is achieved. We obtain the best fit of the data with a distance of 0.77 Mpc, in agreement with the studies by Richer et al. (2001) and Sanna et al. (2008a).

5.4 The SFH of IC10

We adopted the SFH for IC10 published by Weisz et al. (2014), shown in Fig. 3. The grey region delimits the lower and upper limits given by the authors. The plane is divided into four regions, according to the metallicity and the mass of the stars formed at different times, from the present day to ∼12 Gyr ago. As a first try, we considered the average SFR between the lower and upper limits of Weisz et al. (2014).

The results are shown in Fig. 4, where we compare the observed distribution of stars (left-hand panel) and the synthetic population, reported on the right-hand panel (note that in the latter panel, we also show the observed stars, with light, grey points). In the left-hand panel, we indicate three regions of the plane, coded as A, B, and C. According to our interpretation, region A is populated by stars with a significant IR emission, mainly carbon stars, with a small fraction of core helium-burning stars. In region B, we find bright RSG ($M \geq 12\,M_{\odot}$) and massive AGB stars. Region C is populated by stars of various masses and metallicities, characterized by a negligible IR colour excess, suggesting scarcity of dust in their surroundings.

The comparison with the evolutionary tracks, presented in Fig. 1, shows that only stars older than ∼500 Myr evolve into region A of CMD (see Fig. 5). This is a relevant information to examine in more details the most remote epochs. In particular, the distribution of the tracks (see Fig. 1) shows that the width of the C-stars locus is associated to a spread in the initial mass of the star, hence in the age. A sharply peaked SFH, similar to the one obtained when

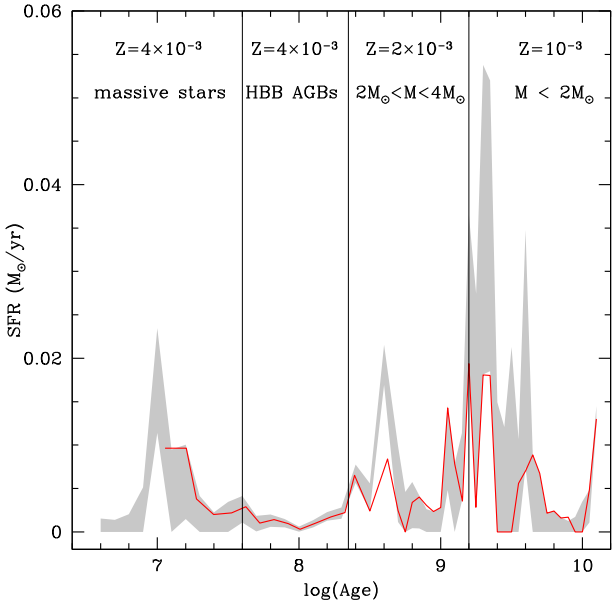

Figure 3. The SFH of IC10 by Weisz et al. (2014) is shown, as a function of the formation epoch of the stars. The grey-shaded area delimits the lower and upper limits. The red line reports the final choice of the SFH that better reproduces the distribution of the data in the colour–magnitude diagrams.

considering the upper limits in Fig. 3, would reflect into a narrow distribution of stars in the CMD, as shown in Fig. 4: we note a strong concentration around the track of ∼1.3 $M_\odot$ stars, determined by the peak in the SFH, which would have occurred ∼2 Gyr ago. On the contrary, we see in the left-hand panel of Fig. 4 a spread in [4.5] slightly in excess of 1 mag, significantly higher than the typical photometric error, which is below 0.1 mag for the stars populating the region of the CMD at $K - [4.5] > 1$. This is consistent with a more uniform SFR across the age interval of 1–5 Gyr, as indicated by the red line in Fig. 3.

We refined the SFH relying on the relative fractions of stars in different colours and magnitude bins and on the number counts of stars in the A–B–C zones of CMD. Looking at the comparison between the data and the theoretical population, a general agreement is found considering the limits suggested for the SFH. Nevertheless, the specific analysis computed in this work allows a more detailed refinement of the SFR, particularly in some age intervals. The main result of this analysis is the determination of the SFH for IC10, represented by the red line in Fig. 3.

The epochs between 300 Myr and 1 Gyr ago are characterized by the formation of stars with mass in the range 2–3 $M_\odot$, which reach the C-star stage during their AGB phase, similarly to their lower mass counterparts. As discussed in Section 4, this class of objects is expected to reach extremely red IR colours (see bottom, left-hand panel of Fig. 2) in the very final AGB phases. The data suggest that only a very small number of objects exhibit such a strong IR emission, thus indicating that the SFR was not significant in those epochs: our simulations suggest that the SFR must have been below 10^{-2} $M_\odot$ yr^{-1} in the 300-Myr–1-Gyr age interval. This is consistent with the prediction by Weisz et al. (2014), apart from the higher peak at ∼400 Myr found by the authors.

In agreement with the recommended values by Weisz et al. (2014), we find that the epochs between 40 Myr and 200 Myr ago were characterized by poor star formation. This is the formation epoch of stars of mass in the range of 4–8 $M_\odot$, which are expected to achieve copious production of silicates during the hot bottom burning (hereafter HBB) phase, reaching a significant degree of obscuration (Ventura et al. 2014). A large SFR in those epochs would reflect into the presence in CMD of bright, obscured stars. The lack of stars in the region of CMD included between the tracks of the 2.5 $M_\odot$ and 7.5 $M_\odot$ models, shown in Fig. 1, indicates that only a very small number of these stars are currently evolving in IC10 (see region B in Fig. 4).

As stated previously, IC10 is generally believed to have been recently exposed to significant star formation, which might be still active. It is therefore important to understand whether the data set used here can add some information on the star-formation activity in recent epochs, earlier than ∼40 Myr. We find that an estimate of the rate with which stellar formation occurred in recent times can be obtained by taking into account the group of stars populating the region $0 < K - [4.5] < 0.5$, $[4.5] \sim 16$ in the CMD. We left on purpose these sources out of regions A, B, and C in Fig. 4, because, as shown in Fig. 1, their position in the plane is consistent both with stars of mass in the range 2.5–3 $M_\odot$ and with RSG stars with masses 9–11 $M_\odot$. In the former case, we should expect that significant star formation occurred 250–600 Myr ago; however, the magnitude spread and the colour extension of the locus of carbon stars populating region A indicate that only a limited number of 2.5–3 $M_\odot$ stars are currently evolving in IC10 (see point iii in Section 4); therefore, we suggest that these objects are RSG stars. Our simulations indicate that the data can be reproduced by assuming significant star formation, with rates of the order of 10^{-2} $M_\odot$ yr^{-1}, between 20 and 30 Myr ago, in excellent agreement with the values given in Weisz et al. (2014).

6 THE EVOLVED STELLAR POPULATION OF IC10

Based on the choices regarding reddening, distance, and SFH discussed in the previous section, we used a population synthesis approach to obtain the expected distribution of the evolved stars in the CMD of IC10. The results from modelling are shown in the right-hand panel of Fig. 5 and compared with the observed points (grey points). We may characterize the stars observed according to their position on the CMD, which is related to the mass of the progenitors and the evolutionary status. We divide the stars in the groups discussed below.

6.1 Carbon stars

Region A in the CMD is predominantly populated by low-mass AGB stars during the C-star phase. These sources are the progeny of 1–2.5 $M_\odot$ stars, formed between ∼500 Myr and 6 Gyr ago.

The mass histogram of the progenitors of these stars, indicated with a solid line in the right-hand panel of Fig. 6, shows a mass distribution extending from ∼1 $M_\odot$ to ∼3 $M_\odot$, with a main peak around ∼1.2–1.3 $M_\odot$, a consequence of the maximum in the SFH that occurred around ∼2.5 Gyr ago (see Fig. 3). Secondary peaks in the mass distribution of the progenitors of these stars are found at ∼1.75 $M_\odot$ and ∼3 $M_\odot$, due to the star-formation activity that took place, respectively, 1Gyr and 300 Myr ago.

The stars populating region A with $1 < K - [4.5] < 2.5$ are experiencing the last TPs, before entering the PNe phase. The surface C/O ratio is in the range $5 < C/O < 10$ (see Fig. 2). The current mass

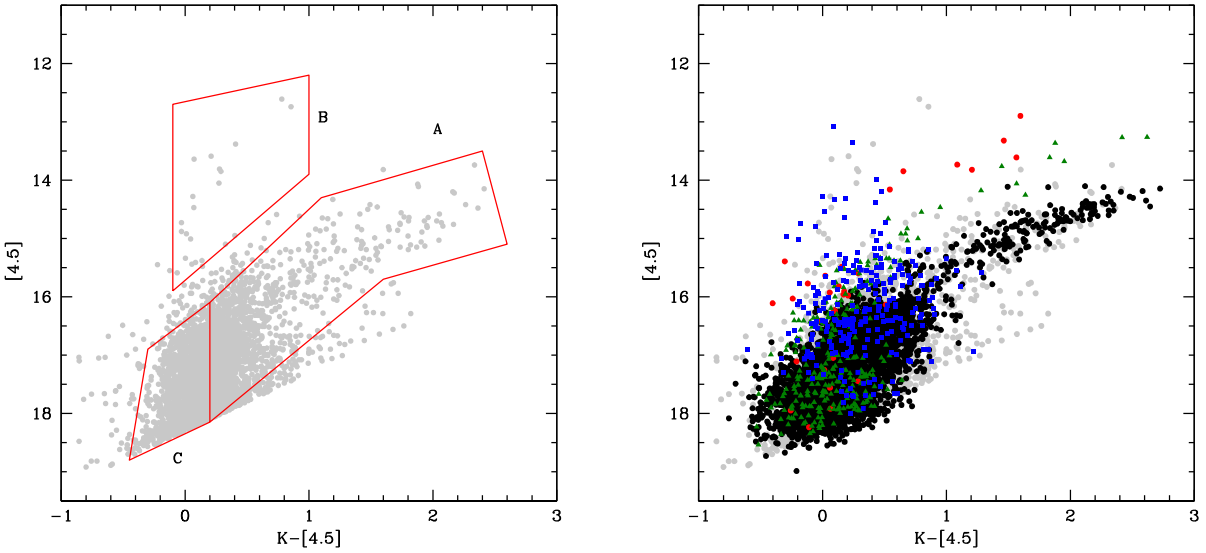

Figure 4. Left: The distribution of IC10 stars in the colour–magnitude ($K - [4.5]$, [4.5]) plane. Right: The results from population synthesis, obtained by adopting the recommended SFH by Weisz et al. (2014). The different colours indicate stars of metallicity $Z = 10^{-3}$ (black points, initial masses below 2 $M_\odot$), $Z = 2 \times 10^{-3}$ (green triangles, descending from stars of mass 2 $M_\odot < M < 4\,M_\odot$), $Z = 4 \times 10^{-3}$ (red points, initial mass above 4 $M_\odot$), and core helium-burning stars (blue squares, also assumed to have a metallicity $Z = 4 \times 10^{-3}$). The observed sample is also shown as light-grey points in the right-hand panel.

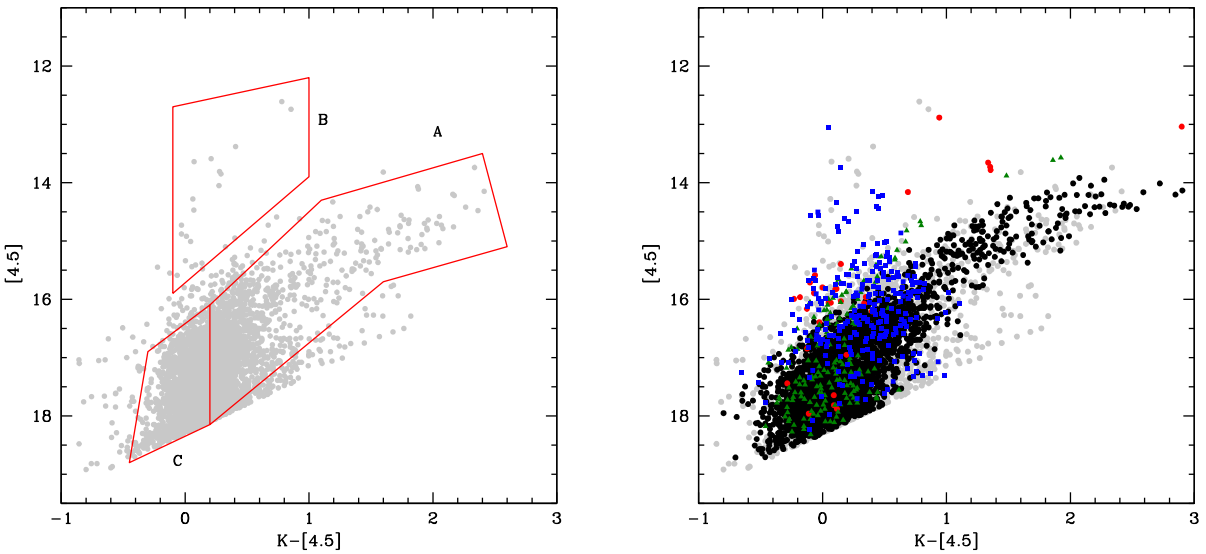

Figure 5. The same as Fig. 4, with the difference that here the synthetic population is obtained by using the SFH represented by the red line in Fig. 3. The meaning of the different colours and symbols is the same as Fig. 4.

of these sources spans the interval 0.6–0.7 $M_\odot$. Although the interpretation of these observations is partly affected by the photometric uncertainties, we predict that brighter stars are of higher initial mass (c.f Fig. 1), because higher mass stars are brighter during these late AGB phases. A small fraction of stars (< 1 per cent of the entire sample) populate the area below region A, with $1 < K - [4.5] < 2$. From a deeper inspection based on different colour–magnitude planes, they are probably residual unresolved foreground sources, background galaxies, and young stellar objects (Boyer et al. 2011). The lack of photometric measurements with filters at wavelengths longer than 4.5 μm (e.g. (J-[8]) affects the possibility to further reduce this contamination.

Region A is also populated by RSG stars of mass in the range 6–9 $M_\odot$ (see the shaded region in Fig. 1). The expected number of these objects within the box delimiting region A partly depends on the assumptions regarding the optical depth. With the present hypothesis on τ_{10}, discussed in Section 3, we find that the percentage of core helium-burning stars in region A is ∼5 per cent. The choice of smaller optical depths would lead to a smaller fraction of core helium-burning stars in this zone of the CMD.

Independently of the τ_{10} choice, the dominant population of stars in region A is made up of low-mass, carbon stars. Although the expected number of core helium-burning stars is small in all cases, exploring this possibility is important to understand whether this

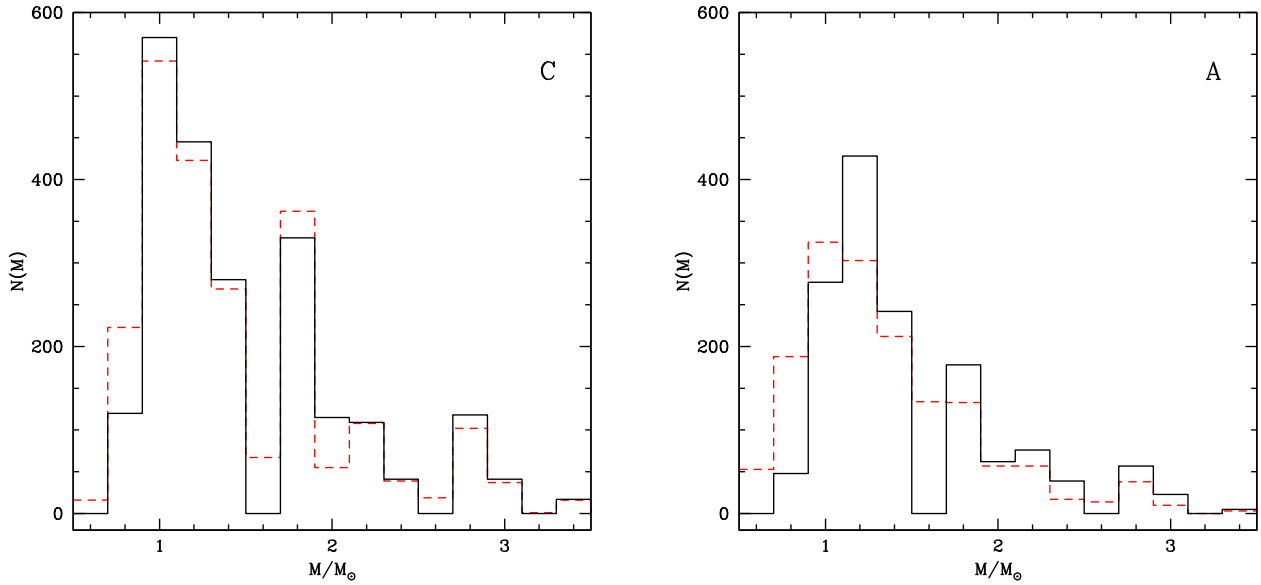

Figure 6. The progenitors mass distribution (black, solid lines) and the current mass (red, dashed) of the stars populating regions C (left-hand panel) and A (right-hand panel) in Fig. 5.

zone of the CMD harbours carbon stars solely, or whether a few obscured O-rich stars surrounded by silicate-type dust are also present.

Region A harbours ∼40 per cent of the overall evolved population of IC10; this result, in agreement with the observations, is consistent with the results shown in Fig. 2 and discussed in Section 4, indicating that low mass, metal-poor stars evolve as carbon stars for almost half of the AGB phase.

6.2 The bright, young stars

The stars populating region B have luminosities above $2 \times 10^4 L_{\odot}$, which rules out the possibility that they are carbon stars (see the top, left-hand panel of Fig. 2). Their magnitudes are compatible either with oxygen-rich AGB stars, descending from $M \geq 4\,\mathrm{M}_{\odot}$ progenitors, currently experiencing HBB, or with RSG stars, with mass in the range of 10–20 $\mathrm{M}_{\odot}$ (see the shaded region in Fig. 1). Selecting between these two possibilities is not obvious. However, we believe that most of the stars evolving into region B, with the exception of the two brightest objects, are RSG stars, based on two arguments:

(i) The stars observed in region B define an approximately vertical sequence, indicating a scarce degree of obscuration; as shown in Fig. 1, this is at odds with the expectations concerning the evolution of massive AGB stars, which produce significant amounts of silicates during the AGB phase (Ventura et al. 2014), thus evolving at redder colours. A possible solution would be that these stars are metal-poor, but this would imply that no metal enrichment occurred in IC10, which seems unlikely.

(ii) As discussed previously, IC10 is known to harbour a relatively young stellar population, as a consequence of high star formation in recent epochs: therefore, the stars in region B are more likely the signature of this recent star-forming activity.

6.3 Scarcely obscured stars

Region C in Fig. 5 harbours stars with a very small degree of obscuration, indicating scarcity of dust in their circumstellar envelope. The progenitor mass distribution, shown in the left-hand panel of Fig. 6, is dominated by low-mass stars, with mass $M \leq 1.5\,\mathrm{M}_{\odot}$.

Compared to the mass distribution of stars evolving to region A, we note a higher fraction of $M < 1\,\mathrm{M}_{\odot}$ objects. This difference occurs because stars of mass below $\sim 1\,\mathrm{M}_{\odot}$ are not expected to reach the C-star stage; thus, they evolve through the AGB phase as oxygen-rich objects, almost dust-free. Note that stars of mass $M \leq 1\,\mathrm{M}_{\odot}$ evolve brighter than the TRGB for only a part of the AGB phase (see the $1\,\mathrm{M}_{\odot}$ model track in Fig. 1); the mass distribution of region C would be more peaked towards the lowest masses otherwise.

We note in the left-hand panel of Fig. 6 that the secondary peaks around $\sim 2\,\mathrm{M}_{\odot}$ and $\sim 3\,\mathrm{M}_{\odot}$ are higher than in region A (right-hand panel). This is because the stars within this range of mass are expected to evolve into region C of the CMD not only in the initial part of the TP-AGB phase, during which little dust is produced, but also for a significant portion of the early AGB phase, also characterized by negligible formation of dust. This is different from their lower mass counterparts, which are expected to evolve brighter than the TRGB (thus within region C) only during the TP-AGB phase.

Region C also involves a modest fraction (below ∼5 per cent) of core helium-burning stars of mass $6\,\mathrm{M}_{\odot} < M < 9\,\mathrm{M}_{\odot}$, with ages younger than 100 Myr.

6.4 Scarcely obscured, bright stars: RSG or low-mass objects?

The analysis of the stars observed in the regions of CMD between zones B and C is particularly tricky, because these sources could descend either from stars with mass in the range of 2.5–3 $\mathrm{M}_{\odot}$, which have just entered the C-star phase (see the track of the $2.5\,\mathrm{M}_{\odot}$ model in Fig. 1), or from RSG stars with mass $9\,\mathrm{M}_{\odot} < M < 11\,\mathrm{M}_{\odot}$ (see the shaded region in Fig. 1).

In the former case, this region of the plane would be populated by stars of mass just below the threshold required to activate HBB, formed between 300 Myr and 1 Gyr ago; this possibility would require a higher SFR in these epochs, compared to the choice shown in Fig. 3. However, we are much more favourable to consider

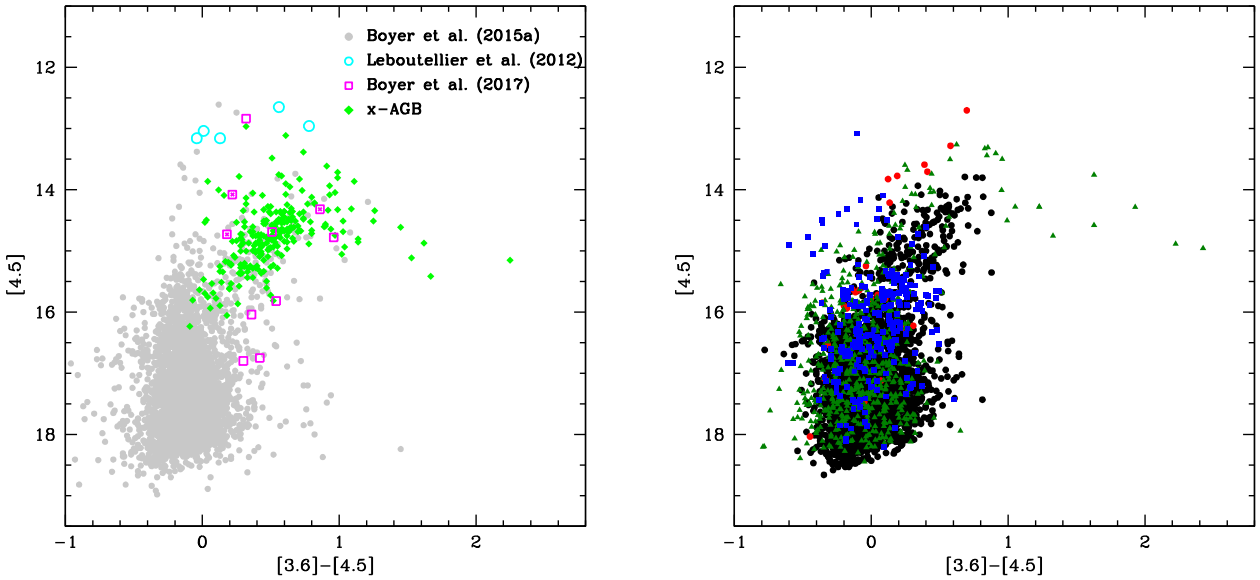

Figure 7. Left: The distribution on the colour–magnitude ([3.6] −[45], [4.5]) plane of the IC10 stars from Boyer et al. (2015a), indicated with grey points. Cyan circles indicate the bright, O-rich stars by Lebouteiller et al. (2012), whereas the obscured stars by Boyer et al. (2017), classified as O-rich, are indicated with magenta squares (crosses inside the square mean variable sources). The x-AGB stars by Boyer et al. (2015b) are represented with light green diamonds. Right: The results from synthetic modelling, with the same symbols used in Figs 4 and 5.

contamination from RSG stars, because: (i) the presence of such class of stars would require the existence of stars brighter than the group of sources populating region A, which is indeed not observed; (ii) stars of mass 2–3 $M_{\odot}$ reach very large degrees of obscuration, which would reflect into a higher fraction of stars at IR colours (see Fig. 1) with respect to the observational evidence.

7 AN ANALYSIS OF OBSCURED STARS IN THE *SPITZER* COLOUR–MAGNITUDE PLANE

To study in a more complete way the population of evolved stars in IC10, we study their distribution on the colour–magnitude ([3.6]−[4.5], [4.5]) plane (hereafter CMDSP). We attempt an analysis similar to the one based on the combined near-IR and *Spitzer* data, done in the previous section on the CMD. This complementary study allows us to consider the RSG, M-type, and xAGB candidates identified by Lebouteiller et al. (2012) and Boyer et al. (2015b, 2017), as described in Section 2.

The left-hand panel of Fig. 7 shows the distribution in the CMDSP of the stars in the sample by Boyer et al. (2015a), the x-AGB stars by Boyer et al. (2015b), the stars studied by Lebouteiller et al. (2012) (only the five stars for which the [4.5] data are available are shown), and the dusty, O-rich sources by Boyer et al. (2017) (we restrict our attention to the 10 sources classified as M-type with a high confidence level). The right-hand panel of Fig. 7 reports the results obtained with our synthetic approach, described in details in the previous sections, used to produce the results shown in the right-hand panel of Fig. 5.

Fig. 8 shows the observations and the results from population synthesis at the same time; to better characterize the obscured stars, we focus on a narrower region of the CMDSP(grey points).

We distinguish a sequence of obscured objects, extending to [3.6]−[4.5] ∼ 1, which we interpret mainly as carbon stars. Furthermore, we note a sequence of bright sources, with [3.6]−[4.5] < 0.3, which corresponds to the stars populating region B in Fig. 5: based on the arguments given in Section 6.2, we believe that the majority

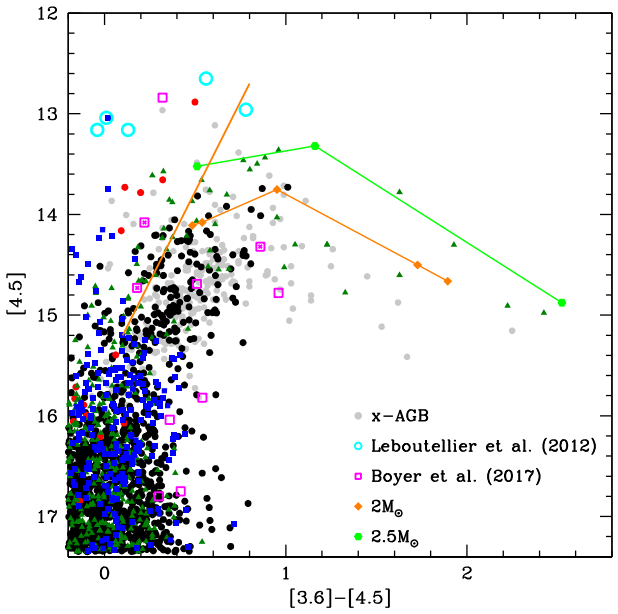

Figure 8. The distribution of IC10 x-AGB stars by Boyer et al. (2015b) (grey points), the stars from Lebouteiller et al. (2012) (cyan circles), and Boyer et al. (2017) (magenta squares) on the colour–magnitude ([3.6] −[45], [4.5]) plane. Results from synthetic modelling are also shown, with the same symbols of Figs 4 and 5. The evolutionary tracks of stars of initial mass 2 $M_{\odot}$ (orange) and 2.5 $M_{\odot}$ (light green) are shown.

of these sources are RSG stars, with a few AGB stars experiencing HBB.

The diagonal, orange line in Fig. 8 can be used to separate carbon stars, expected to be on the right of the line, and their O-rich counterparts, which populate the region on the left. RSG stars can be found both on the left and on the right side of the line. According to our interpretation, the majority (> 90 per cent) of the sources

observed by Boyer et al. (2015b) are carbon stars, descending from low-mass progenitors, of mass in the range of 1–2.5 $M_\odot$.

The stars exhibiting the largest IR emission are of particular interest in the present context, because IC10 harbours the largest number of objects with [3.6]−[4.5] > 1, among all the galaxies in the DUSTiNGS survey (Boyer et al. 2015b). For these sources, which are surrounded by large amounts of dust, the colour provides an indication of the mass of the progenitor, because as far as C-stars are concerned, stars of higher mass reach higher degree of obscuration in the late AGB phases, owing to a larger accumulation of carbon in the surface regions (Ventura et al. 2016). This is partly shown in the right-hand panel of Fig. 7, where we report the tracks in the CMDSP of stars of mass 2, 2.5 $M_\odot$, during the final part of the AGB evolution; lower mass stars do not reach such red colours.

Based on these arguments, we conclude that the stars with the largest degree of obscuration in the Boyer et al. (2015b) sample are the progeny of 2–2.5 $M_\odot$ stars, formed between 500 Myr and 1 Gyr ago. They are evolving through the final AGB phases, after the loss of a significant fraction of their envelope, such that their current mass is in the range of 0.6–0.9 $M_\odot$. The surface regions of these stars are enriched in carbon, owing to the action of repeated TDU events: the surface mass fractions and the C/O ratios are, respectively, $X(C) \sim 0.01$–0.015 and C/O ∼ 3–5. Their large IR colours are determined by the great amounts of dust formed, mainly under the form of solid carbon grains of 0.15–0.25 μm size.

The variable sources by Boyer et al. (2015b) on the left side of the diagonal line are massive AGB stars, currently experiencing HBB. A more detailed characterization of the progenitors is not straightforward in this case, because all the stars of initial mass $M \geq 4\,M_\odot$ evolve to those regions of the CMDSP.

The M-type, dusty stars identified by Boyer et al. (2017), indicated with magenta, open squares, are distributed across the CMDSP (see right-hand panel of Figs 7 and 8), spanning a wide range of colours (0.3 < [3.6]−[4.5] < 1) and magnitudes (12.5 < [4.5] < 17). The five sources with IR colours 0.3 < [3.6]−[4.5] < 0.6 populate a region of the plane distant from the zone covered by the tracks of massive AGB stars. While their colours could be reproduced by invoking a degree of obscuration of AGB stars much larger than the model predictions, their magnitudes are too faint to be considered as stars undergoing HBB. Based on their position on the CMDSP, we may consider the possibility that these sources descend from stars of mass in the range of 7–10 $M_\odot$, currently evolving through the core He-burning phase. This possibility requires a degree of obscuration unusually large for this class of objects of the order of $\tau_{10} \sim 0.2$. Further possibilities to explain these objects are mixed-chemistry sources or binary systems with induced mass loss.

The three stars on the left of the diagonal line in the CMDSP are AGB stars evolving through the HBB phase. For the two faintest objects (#112431 and #118138), this possibility is supported by the DUSTiNGS classification as x-AGB variables. The luminosities of the two sources are compatible with any mass higher than ∼4 $M_\odot$. #105975 is the brightest among this subsample: based on the position on the CMDSP, we conclude that it is a massive AGB star, descending from an $M > 5\,M_\odot$ progenitor. Note that Boyer et al. (2017) claimed a progenitor mass above ∼8 $M_\odot$ for this object. The dissimilarity in this interpretation is due to the higher luminosities achieved by the massive AGB models used in this analysis, determined by the use of the full spectrum of turbulence model for turbulent convection (Canuto & Mazzitelli 1991), which favours stronger HBB conditions (hence higher luminosities) for $M \geq 4\,M_\odot$ stars compared to the models based on the traditional mixing length theory (Ventura & D'Antona 2005; Ventura et al. 2015a).

The interpretation of the two stars from Boyer et al. (2017) with the largest IR colours shown in Fig. 8, namely #121876 and #120247, is more cumbersome, given that their position rules out the possibility that they are massive AGB stars. This conclusion is pretty independent of the details of the dust-formation modelling: our tests show that an artificial increase in the optical depth would lead to small values of [4.5], at least one magnitude brighter than observed. Their colours and magnitudes can be reproduced by RSG models of mass around ∼8–10 $M_\odot$, if an optical depth of $\tau_{10} \sim 1$ is assumed. This very large degree of obscuration might be associated to a strong mass loss occurring during the RSG evolution. For the star #121876, this explanation is at odds with the variability detected. We leave this problem open.

Regarding the five stars analysed by Lebouteiller et al. (2012), for which the combined [3.6] and [4.5] data are available, we see in Fig. 8 that they populate a large luminosity region in the CMDSP, with their [3.6]−[4.5] colours spanning almost 1 mag. The bluer three sources, i.e. #4, #6, and #14, populate the region of the CMDSP where stars of mass around 20 $M_\odot$ evolve during the RSG phase. This understanding is in agreement with the conclusions drawn by Lebouteiller et al. (2012) regarding the nature of these objects. Conversely, the IR fluxes of the redder two stars, #8 and #12, are hardly compatible with an RSG origin. Their colours and luminosities are consistent with massive AGB stars undergoing HBB, with progenitor masses $M \geq 6\,M_\odot$. This conclusion is also supported by the $K - [4.5]$ colours of these two objects, of the order of $K - [4.5] \sim 1.5$, much more consistent with a massive AGB than with an RSG origin (see the track of the 7.5 $M_\odot$ model in Fig. 1).

8 DUST PRODUCTION IN IC10

The analysis done in the previous sections outlined that IC10 harbours a numerous group of carbon stars, with various degrees of obscuration. The increase in the IR emission in these objects is triggered by the formation of solid carbon grains that grow bigger in size. In this context, we may neglect the formation of SiC grains, owing to the low metallicity involved, hence a low Si/C ratio (Sloan et al. 2012; Ventura et al. 2014).

According to our interpretation, the majority of the stars populating region A in the CMD, shown in Fig. 5 as black points, are surrounded by carbon dust grains, whose size reaches ∼0.15 μm in the reddest objects, populating the region of the plane with $K - [4.5] \sim 2.5$. The optical depths of these stars range from $\tau_{10} \sim 0.2$ to $\tau_{10} \sim 1$. While most of the evolved stellar population of IC10 is shown in Fig. 5, the results presented in the previous section and shown in Fig. 7 indicate the presence of a few stars with an extremely large degree of obscuration, which populate the region of CMDSP at 1.5 < [3.6]−[4.5] < 2.5. Some of these sources are not present in the Gerbrandt et al. (2015) sample, owing to their low fluxes in the K band. These stars, classified as extreme AGB by Boyer et al. (2015b), are characterized by optical depths of the order of $\tau_{10} \sim 4$ and are surrounded by carbon grains of ∼0.25 μm size.

The current dust mass loss rates for the AGB stars in the synthetic population of IC10 are shown as a function of the IR colours in Fig. 9. Note that only the stars with rates above 10^{-10} $M_\odot$ yr^{-1} are shown. Thus, the dust mass loss rates by low-mass stars during the initial AGB phases, before becoming carbon stars, are excluded from this figure.

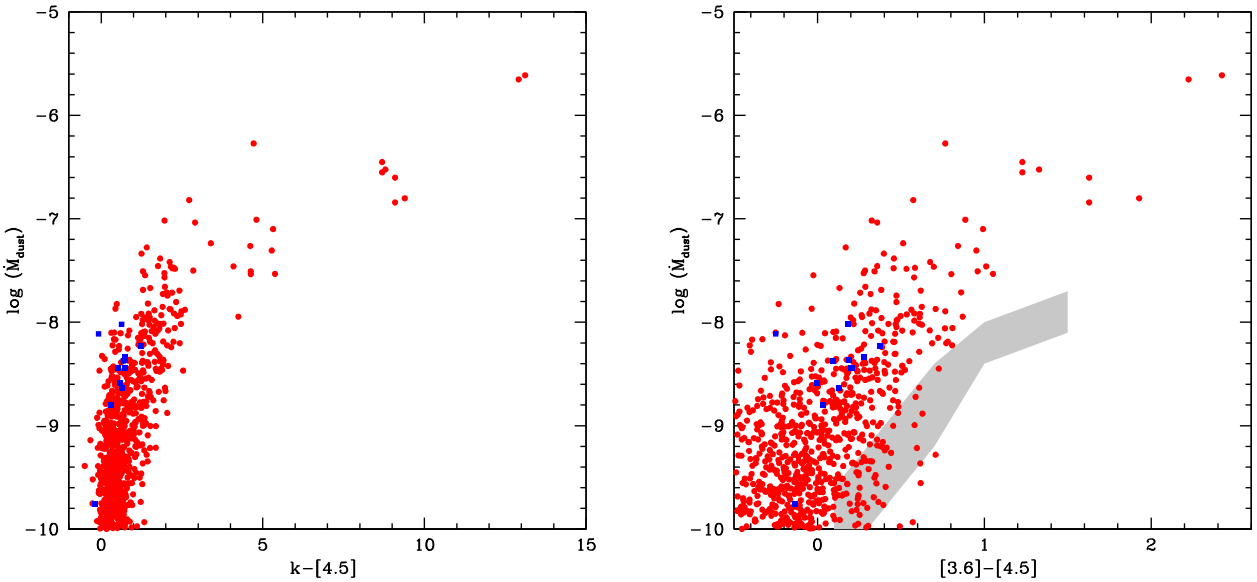

Figure 9. The dust mass loss rate of the stars in our synthetic population, as a function of the $K-[4.5]$ (left-hand panel) and [3.6]−[4.5] (right-hand panel) colours. Red points indicate carbonaceous dust, whereas blue squares indicate silicate and alumina dust production. The grey, shaded region in the right-hand panel indicates the relation for SMC AGB stars, given in Srinivasan et al. (2016).

According to our interpretation, stars populating region A in Fig. 5 eject dust into the interstellar medium with rates in the range of $10^{-8}\,M_\odot/yr^{-1} < \dot{M}_d < 3\times10^{-7}\,M_\odot\,yr^{-1}$. As stated previously, this dust is essentially under the form of solid carbon particles. The stars with the reddest colours are characterized by higher rates, up to $\dot{M}_d \sim 2\times10^{-6}\,M_\odot\,yr^{-1}$.

Fig. 9 (right-hand panel) includes a comparison to the SMC carbon-stars locus from Srinivasan et al. (2016), showing significant differences in the [3.6]−[4.5] > 0.5 domain. Our results for the dust mass loss rates are 5–10 times higher than those given in Srinivasan et al. (2016); more important, the slope of the $\dot{M}_d$ versus [3.6]−[4.5] trend is larger in this study. These dissimilarities mainly reflect the differences in the outflow velocities: while Srinivasan et al. (2016) assume $v_{out} = 10\,km\,s^{-1}$, we find that the speed of the winds changes with the degree of obscuration, ranging from $v_{out} \sim 5$–$10\,km\,s^{-1}$ for the carbon stars with the lowest IR emission to $v_{out} \sim 40$–$50\,km\,s^{-1}$ for the most obscured stars. A further though less relevant factor is Ψ, the dust-to-gas ratio: while Srinivasan et al. (2016) assume $\Psi = 0.005$ for carbon stars, in this study we find that Ψ ranges from 0.002 to 0.01.

The discussion in the previous sections showed that massive AGB stars are present in very modest numbers in IC10. These sources are represented as blue squares in Fig. 9. The overall DPR by this class of objects is therefore negligible when compared to the carbon dust budget. Additional dust, but in negligible quantities, is produced by low-mass stars during the AGB phases previous to the achievement of the carbon-star stage. Regarding RSG stars, we do not have a straight recipe to find out the rate with which they form dust. However, we expect a minor contribution, because these sources trace an almost vertical trend both in the CMD and the CMDSP, thus suggesting that only small quantities of dust are present in their surroundings. This is consistent with the conclusions by Lebouteiller et al. (2012).

Based on the results shown in Fig. 9, we estimate an overall DPR by the evolved stellar population of IC10 of $7\times10^{-6}\,M_\odot\,yr^{-1}$. This dust is mainly composed of solid carbon grains. Silicate particles provide a very small contribution of the order of $10^{-8}\,M_\odot\,yr^{-1}$.

9 THE PNE POPULATION OF IC10

Magrini & Goncalves (2009) discussed the further possibility offered by the analysis of the PNe population to reconstruct the SFH of IC10. In their work, the authors present spectroscopic observations of 12 PNe in IC10, nine out of which were spectroscopically confirmed.

In order to compare our predictions and understanding of the evolved population nowadays evolving in IC10 with the results from Magrini & Goncalves (2009), we rely on the three PNe for which both the N and O abundances are available, namely PN9, PN17, and PN22; given the lack of the carbon mass fractions, the contemporary knowledge of the abundances of these two species is the minimum requirement to achieve any interpretation.

Fig. 10 shows the data by Magrini & Goncalves (2009) in the oxygen versus *N*/*O* plane, compared to our models, for stars of different initial mass and metallicities $Z = 1\times10^{-3}, 2\times10^{-3}$. The trend with mass of the theoretical loci follows a counterclockwise pattern, originated by the relative importance of TDU and HBB during the AGB phase for stars of different mass (Ventura et al. 2015b).

In agreement with the conclusions by Magrini & Goncalves (2009), we rule out the possibility that the three PNe descend from massive progenitors, because the measured *N*/*O*s are not compatible with any contamination from HBB, which would favour a large increase in the N content, hence in the *N*/*O* ratio. This may be consistent with the discussion in Section 6, according to which we expect only a very few massive AGB stars to evolve in IC10. Anyway, the PNe sample is far from being complete or representative; therefore, we cannot draw any conclusion from this evidence.

PN17 is the one with the smallest oxygen among the PNe in the sample. We tentatively suggest that it descends from a low-metallicity progenitor of initial mass around $\sim1.1\,M_\odot$. The chemistry of PN22 and PN9 is compatible with progenitors of slightly higher mass of the order of ~1.3–$1.5\,M_\odot$. This understanding is further supported by the observed fluxes from these objects. To this aim, we extended the evolutionary tracks until the beginning

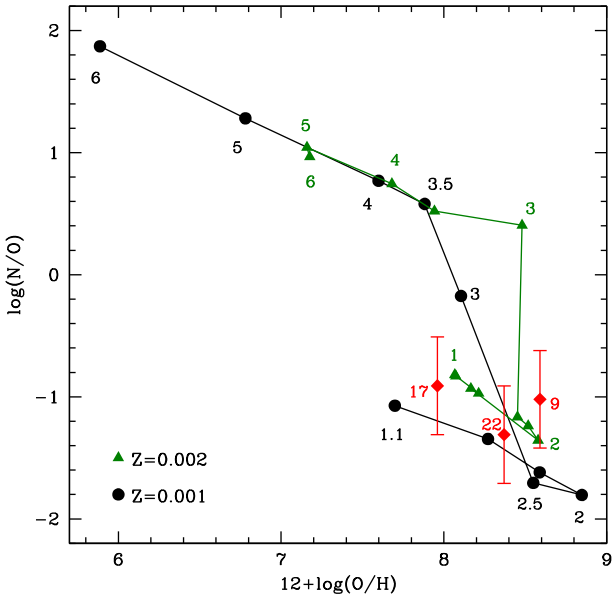

Figure 10. Red diamonds indicate the chemical composition of the 3 PNe in IC10 studied by Magrini & Goncalves (2009) for which both the O and N measurements are available. Black points and green triangles point the final chemistry of AGB models of mass in the range of 1–6 $M_\odot$ and metallicity, respectively, $Z = 10^{-3}$ and $Z = 2 \times 10^{-3}$.

of the WD cooling (Ventura et al. in preparation) and verified that the post-AGB luminosities of 1.1 $M_\odot$ and 1.5 $M_\odot$ stars differ by $\delta \log L = 0.3$. This is in agreement with the fact that the relative fluxes observed at $\lambda = 5007$Å given by Magrini & Goncalves (2009) are $\log(F_{PN9}/F_{PN17}) = 0.27$ and $\log(F_{PN22}/F_{PN17}) = 0.21$.

10 CONCLUSIONS

We study the conspicuous evolved stellar population of the starburst galaxy IC10, with the aim of characterizing the individual sources observed in terms of mass, age, and chemical composition and to reconstruct the SFH of the galaxy. We use stellar models evolved through the AGB phase, which also include the description of the dust-formation mechanism. This step is crucial to interpret the SED and the colours of these objects, because the dust in their circumstellar envelopes reprocesses the radiation emitted by the central star to IR wavelengths.

The analysis is based on the combination of IR and mid-IR fluxes of a sample of stars, obtained by cross-correlating different catalogues. The distribution of the stars in the $(J - K, K - [4.5])$ and $(K - [4.5], [4.5])$ planes allows the evaluation of the reddening and distance of the galaxy: we obtain $E(B - V) = 1.85$ mag and $d = 0.77$ Mpc, within the range of values reported in the literature.

The analysis of the overall distribution of stars in the $(K - [4.5], [4.5])$ plane indicates that ∼40 per cent of the IC10 stars brighter than the TRGB are carbon stars, descending from 1–2.5 $M_\odot$ progenitors. The majority of these objects descend from 1.1–1.3 $M_\odot$ stars, formed during the major epoch of star formation, which occurred around 2.5 Gyr ago. The scarcity of stars in the region of the plane covered by oxygen-rich, massive AGB stars, experiencing HBB, indicates low star formation between 40 and 200 Myr ago. The presence of bright stars in the observed distribution can be reproduced by invoking significant star formation, of the order of 10^{-2} $M_\odot$ yr^{-1}, in recent times (<40 Myr); this is consistent with the fact that IC10 is considered as a starburst galaxy.

The stars with the largest IR emission, characterized by extremely low NIR fluxes, are present only in the *Spitzer* sample. Though few in number, accounting for the presence of these objects is important for a correct determination of the current DPR in IC10. The comparison with the models suggests that these extremely red sources are carbon stars, descending from 2–2.5 $M_\odot$ stars, and are evolving through the very final AGB phases. Their large degree of obscuration is due to the presence of significant quantities of carbon dust in their winds, with grains of 0.2–0.25 μm size. These stars provide the largest contribution to the dust nowadays ejected into the interstellar medium of this galaxy, with DPR above 10^{-7} $M_\odot$ yr^{-1}. We estimate that the overall DPR of IC10, largely dominated by carbon stars, is 7×10^{-6} $M_\odot$ yr^{-1}.

This work further confirms that the IR study of the evolved population of galaxies is a promising tool to analyse the stellar content of the host system, to reconstruct the SFH, and to provide a determination of the reddening and distance. This is a welcome result under the light of the upcoming launch of the *JWST* that will significantly enlarge the volume of dwarf galaxies where bright and evolved stellar populations will be accessible.

ACKNOWLEDGEMENTS

The authors are indebted to the anonymous referee for the careful reading of the paper and for the several suggestions and comments that helped improving significantly the quality and the clarity of the manuscript. FDA and DAGH acknowledge support provided by the Spanish Ministry of Economy and Competitiveness (MINECO) under grant AYA-2017-88254-P.

REFERENCES

Bladh S., Höfner S., 2012, A&A, 546, A76
Bladh S., Höfner S., Nowotny W., Aringer B., Eriksson K., 2013, A&A, 553, A20
Bladh S., Höfner S., Aringer B., Eriksson K., 2015, A&A, 575, A105
Bladh S., Paladini C., Höfner S., Aringer B., 2017, A&A, 607, A27
Boyer M. L. et al., 2011, AJ, 142, 103
Boyer M. L. et al., 2015a, ApJS, 216, 10
Boyer M. L. et al., 2015b, ApJ, 800, 51
Boyer M. L., McDonald I., Srinivasan S., Zijlstra A., van Loon J. T., Olsen K. A. G., Sonneborn G., 2015c, ApJ, 810, 116
Boyer M. L. et al., 2017, ApJ, 851, 152
Canuto V. M. C., Mazzitelli I., 1991, ApJ, 370, 295
Chieffi A., Limongi M., 2013, ApJ, 764, 21
Dell'Agli F., Ventura P., García-Hernández D. A., Schneider R., Di Criscienzo M., Brocato E., D'Antona F., Rossi C., 2014, MNRAS, 442, L38
Dell'Agli F., Ventura P., Schneider R., Di Criscienzo M., García-Hernández D. A., Rossi C., Brocato E., 2015a, MNRAS, 447, 2992
Dell'Agli F., García-Hernández D. A., Ventura P., Schneider R., Di Criscienzo M., Rossi C., 2015b, MNRAS, 454, 4235
Dell'Agli F., Di Criscienzo M., Boyer M. L., García-Hernández D. A., 2016, MNRAS, 460, 4230
Demers S., Battinelli P., Letarte B., 2004, A&A, 424, 125
Ferrarotti A. D., Gail H. P., 2006, A&A, 553, 576
Gerbrandt S. A. N., McConnachie A. W., Irwin M., 2015, MNRAS, 454, 1000
Gonçalves D. R., Teodorescu A. M., Alves-Brito A., Méndez R. H., Magrini L., 2012, MNRAS, 425, 2557
Groenewegen M. A. T., Sloan G. C., 2018, A&A, 609, 114
Groenewegen M. A. T. et al., 2007, MNRAS, 376, 313
Groenewegen M. A. T., Sloan G. C., Soszyński I., Petersen E. A., 2009, A&A, 506, 1277

Gruendl R. A., Chu Y.-H., Seale J. P., Matsuura M., Speck A. K., Sloan G. C., Looney L. W., 2008, ApJ, 688, L9
Hamedani Golshan R., Javadi A., van Loon J. T., Khosroshahi H., Saremi E., 2017, MNRAS, 466, 1764
Javadi A., van Loon J. T., Khosroshahi H. G., Tabatabaei F., Hamedani Golshan R., Rashidi M., 2017, MNRAS, 464, 2103
Jones O. C., Meixner M., Sargent B. A., Boyer M. L., Sewiło M., Hony S., Roman-Duval J., 2015, ApJ, 811, 145
Jones O. C., Meixner M., Justtanont K., Glasse A., 2017, ApJ, 841, 15
Karakas A. I., Lattanzio J. C., 2014, PASA, 31, e030
Kennicutt R. C., Jr, Lee J. C., Funes J. G. J. S., Sakai S., Akiyama S., 2008, ApJS, 178, 247
Kim M., Kim E., Hwang N., Lee M. G., Im M., Karoji H., Noumaru J., Tanaka I., 2009, ApJ, 703, 816
Kraemer K. E., Sloan G. C., Wood P. R., Jones O. C., Egan M. P., 2017, ApJ, 834, 185
Lagadec E., Zijlstra A. A., 2008, MNRAS, 390, L59
Lebouteiller V. et al., 2012, A&A, 546, A94
Magrini L., Goncalves R., 2009, MNRAS, 398, 280
Massey P., Armandroff T. E., 1995, AJ, 109, 2470
Massey P., Holmes S., 2002, ApJ, 580, L35
Massey P., Armandroff T. E., Conti P. S., 1992, AJ, 103, 1159
Mateo M. L., 1998, ARA&A, 36, 435
McDonald I., White J. R., Zijlstra A. A., Guzman Ramirez L., Szyszka C., van Loon J. Th., Lagadec E., Jones O. C., 2012, MNRAS, 427, 2647
Nanni A., Bressan A., Marigo P., Girardi L., 2013, MNRAS, 434, 2390
Nanni A., Bressan A., Marigo P., Girardi L., 2014, MNRAS, 438, 2328
Nanni A., Marigo P., Groenewegen M. A. T., Aringer B., Girardi L., Pastorelli G., Bressan A., Bladh S., 2016, MNRAS, 462, 1215
Nanni A., Marigo P., Girardi L., Rubele S., Bressan A., Groenewegen M. A. T., Pastorelli G., Aringer B., 2018, MNRAS, 473, 5492
Nenkova M., Ivezić Ž., Elitzur M., 1999, in Sprague A., Lynch D. K., Sitko M., eds, *LPIContributions 969, Workshop on Thermal Emission Spectroscopy and Analysis of Dust, Disks, and Regoliths*, Lunar and Planetary Institute, Houston, TX, p. 20
Ramstedt S. et al., 2014, A&A, 570, L14
Rau G., Paladini C., Hron J., Aringer B., Groenewegen M. A. T., Nowotny, 2015, A&A, 583, A106
Richards A. M. S. et al., 2014, A&A, 572, L9
Richer M. G. et al., 2001, A&A, 370, 34
Sakai S., Madore B. F., Freedman W. L., 1999, ApJ, 511, 671
Salpeter E. E., 1955, ApJ, 121, 161
Sanna N. et al., 2008a, Mem. Soc. Astron. Ital., 79, 747
Sanna N. et al., 2008b, ApJ, 688, L69
Sanna N. et al., 2009, ApJ, 699, L84
Schlafly E. F., Finkbeiner D. P., 2011, ApJ, 737, 103
Sloan G. C. et al., 2012, ApJ, 752, 140
Srinivasan S., Boyer M. L., Kemper F., Meixner M., Sargent B. A., Riebel D., 2016, MNRAS, 457, 2814
Tehrani K., Crowther P. A., Archer I., 2017, MNRAS, 472, 4618
Vacca W. D., Sheehy C. D., Graham J. R., 2007, ApJ, 662, 272
Vaduvescu O., McCall M. L., Richer M. G., 2007, AJ, 134, 604
Ventura P., D'Antona F., 2005, A&A, 431, 279
Ventura P., Zeppieri A., Mazzitelli I., D'Antona F., 1998, A&A, 334, 953
Ventura P. et al., 2012a, MNRAS, 420, 1442
Ventura P. et al., 2012b, MNRAS, 424, 2345
Ventura P., Karakas A. I., Dell'Agli F., Boyer M. L., García-Hernández D. A., Di Criscienzo M., Schneider R., 2015a, MNRAS, 450, 3181
Ventura P., Stanghellini L., Dell'Agli F., García-Hernández D. A., Di Criscienzo M., 2015b, MNRAS, 452, 3679
Ventura P., Karakas A. I., Dell'Agli F., García-Hernández D. A., Boyer M. L., Di Criscienzo M., 2016, MNRAS, 457, 1456
Ventura P., Karakas A., Dell'Agli F., García-Hernández D. A., Guzman-Ramirez L., 2018, MNRAS, 475, 2282
Ventura P., Dell'Agli F., Di Criscienzo M., Schneider R., Rossi C., La Franca F., Gallerani S., Valiante R., 2014, MNRAS, 439, 977
Weisz D. R., Dolphin A. E., Skillman E. D., Holtzman J., Gilbert K. M., Dalcanton J. J., Williams B. F., 2014, ApJ, 789, 147
Woods P. M. et al., 2011, MNRAS, 411, 1597

This paper has been typeset from a TEX/LATEX file prepared by the author.